Hydraulic of rock-ramp fishway with lateral slope

Ludovic Cassan, Flavia C Miranda, Pascale Laurens, Dominique Courret

Environmental Fluid Mechanics
https://doi.org/10.1007/s10652-023-09958-6

ORIGINAL ARTICLE

Hydraulic of rock-ramp fishway with lateral slope

Ludovic Cassan[1] · Flavia C. Miranda[1] · Pascale Laurens[1] · Dominique Courret[2]

Received: 22 February 2023 / Accepted: 13 October 2023

Abstract

For an efficient restoration of ecological continuity, rock-ramp fishways with protruding blocks and lateral slope can allow to conciliate two opposite objectives: sufficiently low flow velocities in some parts of the ramp for fish passage and a large global discharge for attractiveness. Flows in such ramps with several lateral slopes (from 5% to 18.5%), longitudinal slopes (from 1% to 7%) and discharges were investigated experimentally on a one-fifth scale model and numerically with RANS and LES models, to check up their passability compared to ramps with no lateral slope. Results revealed that the methodology for assessing stage-discharge relationship and maximum velocities is still relevant whatever the lateral slope. However, as the lateral slope increases, so does the lateral deviation of the free surface, as well as the transverse and vertical velocities in the emergent part of the ramp, near the submerged part. This is why it appears preferable to limit the transversal slope to a maximum 12% in rock-ramp fishways with protruding blocks. This recommendation is already much higher than the one applied up to now in France (lower or equal to the longitudinal slope, so mostly lower or equal to 4% to 6%) and will allow to reduce the width and thus the cost of the ramp.

Highlights

- CFD simulation with LES is pertinent to investigate flow in rock-rampfishway with a transversal slope and protruding blocks either emergent orsubmerged.
- Lateral slope up to 12% do not disturb flow in the part where blocks areemergent, which makes it possible to consider lower build-cost fishway.

✉ Ludovic Cassan
lcassan@imft.fr

Flavia C. Miranda
fcavalcantim@gmail.com

Pascale Laurens
laurens@imft.fr

Dominique Courret
dominique.courret@ofb.gouv.fr

[1] CNRS, IMFT, University of Toulouse, Allée du Pr. Camille Soula, 31400 Toulouse, France

[2] OFB, Pôle Écohydraulique, Allée du Pr. Camille Soula, 31400 Toulouse, France

Published online: 07 November 2023

- Design procedure for rock-ramp fishway remains valid with lateral slopeswith some precautions.

Keywords Rock-ramp · Fishway · Drag coefficient · Lateral slope

1 Introduction

In order to restore efficiently fish passage at low head weirs, rock-ramps with protruding macro-roughness are hydraulic devices showing many advantages when implemented with a lateral slope (Fig. 1): (1) a progressive evolution of the water depths and velocities over the width of the ramp, which is interesting for fish passage for a wide range of species, and (2) the possibility of transiting high flows essentially thanks to the deepest parts of the ramp, which is interesting for its attractiveness. In addition, the lateral slope is useful to manage the variations of upstream water levels from low to high river flows, while keeping emerging blocks on a part of the ramp.

Several design laws for these structures have already been proposed for different forms of obstacles [8, 15] or for natural blocks [3]. However they are based on a description of the flow with a horizontal bed in the transverse direction of the flow. Even though a lateral slope may be considered, the stage-discharge relationship is always calculated assuming negligible lateral transfers. In France, the assumption is still taken as a precaution that the lateral slope is less or equal to the longitudinal one, which mostly varies between 4 % and 6 % depending on the target species [14]. However, the option of using higher values to the lateral slope would be interesting. For a given variation of the upstream water level to maintain, this would reduce the ramp width and consequently its building cost, while maintaining an equivalent flow rate that ensures its attractiveness. It is therefore necessary to verify if lateral transfers induced by lateral slopes have a negative effect on the flow conditions inside the ramp and on the fish passage.

In France, the passability of rock-ramps with protruding macro-roughness is assessed according to 3 criteria [5, 14]:

- A maximum value for the maximum velocity of jet between blocks, varying between 1.5 and 2.5 *m/s* depending on target species
- A minimum value for the water depth, varying between 0.2 and 0.4 m
- And a maximum value for the volumetric dissipated power, varying between 200 and 500 W/m^3

Fig. 1 Rock-ramp fishway with a longitudinal and lateral slope set at 5 %. Blocks have a constant 60 cm height and 50 cm diameter

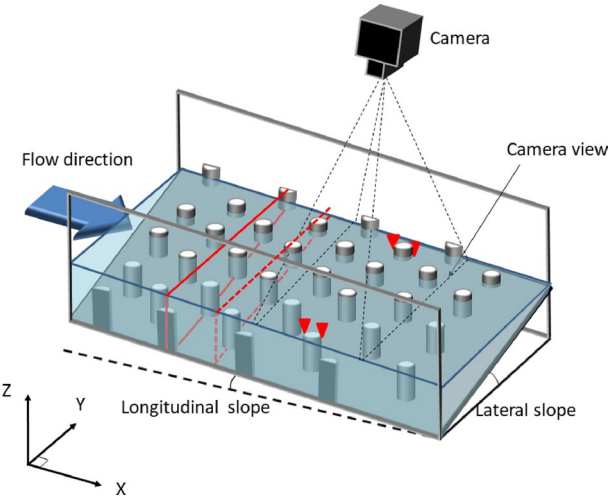

Fig. 2 Schematic 3D view of the experimental device. Red triangles represent the water level measurement location. Red lines show planes drawn on Fig. 3

It is assumed that the fish passage of the same fishpass with no lateral slope has already been investigated [3, 21]. Then the study focuses on the difference in flow patterns induced by the lateral slope, in particular concerning design process.

The study was conducted both experimentally on a one-fifth scale model and numerically with RANS and LES models. Ramps with several lateral slopes (5% and 18.5%), longitudinal slopes (from 1% to 7%) and discharges were investigated. CFD simulations were also performed for a lateral slope of 12%. Experiments allowed to highlight the lateral slope influence on the free surface and the velocities, and to verify the stage-discharge laws. CFD simulation validated on some experiments were performed to explore the velocity fields, as such simulations have been successfully implemented for similar flow around blocks with large Froude number [9, 12, 15] and are expected to provide realistic calculations even for submerged blocks.

2 Experimental devices

2.1 Scale model and configuration

The experimental channel was 1 m wide and 14 m long. The walls were made of Plexiglas and glass. The channel could be tilted up to a slope of 10 %. A removable PVC bottom allowed to impose a 6 m long lateral slope. The tested lateral slopes are 5 % and 18.5 % (Fig. 2). The block are circular, which corresponds to a large majority of rock-ramp fishpass in France. However, it is the most disadvantageous shape to obtain sufficiently low passing speeds [6, 15]. In the following, lengths, distances and discharges are the scaled values and not prototype ones.

An arrangement of cylindrical blocks was positioned in a staggered pattern, the distance between the centers of the blocks is noted a_y in the transverse direction and a_x in the longitudinal direction. For the 3 configurations the bottom is smooth due to a PVC blade on the bed. The density of blocks is defined by a surface density (concentration) and noted C. The transverse dimension of the block facing the flow is noted D (equal to the diameter for a

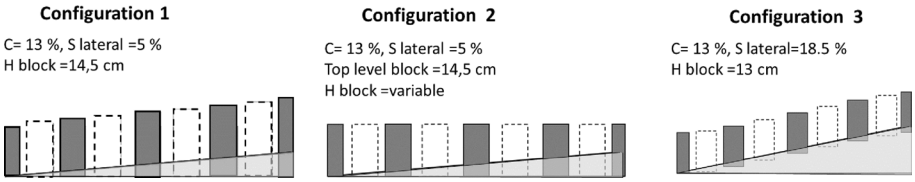

Fig. 3 Experimental configurations used, viewed in a transversal plane. Dot-line represent blocks in the following rows

Table 1 Geometrical and hydrodynamic characteristics of studied cases

	Config.	Long. slope (%)	Lat. slope (%)	Q (l/s)	h (m)
Experiment	1	3, 5 and 7	5	50–200	0.1–0.2
	2	1–7	5	10–200	0.05–0.22
	3	1–7	18.5	50–200	0.18–0.3
Simulation	2	5	5	50	0.11
	3	5	18.5	100, 180	0.22, 0.278
	4	5	12	100, 180	0.19, 0.23

Configuration 4 is only for simulation. Water depths for simulations are those imposed to reproduce experimental cases (only 50, 100 or 180 l/s)

circular pad). Thus the concentration is obtained by the ratio $C = D^2/a_x a_y$. The diameter of all obstacles is 9 cm. They were all positioned so as to be perpendicular to the longitudinal slope. Concerning the height of the blocks, they depend on the geometrical configurations. They are specified below and described on Fig. 3.

- Configuration 1: the spacing $a_x = a_y$ is 25 cm. The concentration is therefore 13%. The height of the blocks in their center is 14.5 cm. The lateral slope is 5 %.
- Configuration 2: the spacing $a_x = a_y$ is 25 cm. The concentration is 13%. The lateral slope is 5 %. Compared to configuration 1, the top of the block is identical for all the blocks in the same row. Therefore, all the blocks will be submerged at the same time for a given water level.
- Configuration 3: the spacing $a_x = a_y$ is 25 cm. The concentration is 13%. The lateral slope is now 18.5 %. The height of the blocks at their center is 13 cm.

For configurations 1, 2, and 3, water depth measurements were made for longitudinal slopes ranging from 1% to 7%. The flows varied globally from 20 to 160 l/s. A geometrical configuration with a specific slope and discharge is named as an experimental case in the following. Depending on the longitudinal slope, some flows giving too many impassable conditions were not tested because the corresponding in situ velocity is superior to 3 m/s, or water depth in the shallower passage is lower than 20 cm (4 cm on scale model). Flow rates were measured with an ultrasonic flow meter (Fluxus ADM 5107) placed on the pump discharge line with an accuracy of 2 to 5%. The longitudinal slope was measured with an electronic inclinometer (Bosch DNM120 L).

Table 1 summarizes experiments and simulations done for this study. For all cases, water depths are measured but free surface velocity was only measured for cases with configurations 2 and 3.

2.2 Water level measurement

Water levels were measured with a point gauge and a ruler. The measurement points were located upstream and downstream of the extreme right and left blocks. For cases where the blocks were submerged, only the measurement downstream of the emerged block was made. A measured point was also added at the minimum cross-section location. In previous studies, it was shown that the average height over an area $a_x * a_y$ around a block can be accurately estimated by averaging the upstream and downstream water depths on the block [6]. Compared to previous studies without lateral slope, the average height around a block can be different on the right and left sides of the channel. There may therefore be a lateral inclination of the free surface.

The water depths were measured at the blocks line located 3 ms from the channel entrance, in the middle of the section with a lateral slope. The measurements were repeated on 2 or 3 consecutive rows to check the uniformity of the flow. We will present hereafter the sole central row measurements.

2.3 Particle tracking velocimetry

In order to obtain spatialized velocity measurements for all the experiments, an optical measurement device has been implemented. A Canon E600D camera was placed above the flow. It allowed to take videos of the flow at a frequency of 50 frames/second with a resolution of 1920*1080 pixels. The measured field was set to cover the entire width of the flow. The resolution was therefore around 1 pixel/mm, but it was adjusted for each experiment using an orthorectification of the images performed with openCV python Library.

The flow was seeded with 3–4 cm diameter corn chips. These particles were identified on each image. The velocity was obtained by measuring the displacement of a chip between 2 images. To detect the chips and to associate them 2 by 2 between images, we used the algorithms developed at IMFT [12, 18]. For each experiment, the velocity fields were thus averaged over 30 s. The velocities were also spatially averaged over areas of 20 pixels on each direction.

3 Numerical simulation

Configurations 2 and 3 were simulated with a longitudinal slope of 5 % in order to obtain a knowledge of the flows over the entire water depth. An intermediate configuration with a 12 % lateral slope is also simulated.

The longitudinal slope effect was applied by decomposing the gravity into longitudinal $g\sin(\theta)$ and vertical $g\cos(\theta)$ components, with $\theta = \arctan(S)$ and S the considered slope.

The simulations were performed using the two-phase flow solver interFoam of the open source C++ library OpenFOAM v1812. It solves the Navier–Stokes equations by applying the pressure–velocity PIMPLE (merged PISO-SIMPLE) correction procedure. For turbulence modeling, this study employed LES with the subgrid-scale model Smagorinsky [20] and the RANS model K-omega SST [16].

The different simulated cases are shown in Table 2. The hydrodynamic conditions are imposed numerically with an initial water volume which is conserved along all the simulation. Then the averaged water level remains constant. As the experimental cases are defined with a given discharge, the comparison between experiment and numerical results needs to

Table 2 Parameters of the numerically studied cases

Num. case	Lateral slope (%)	h (m)	Turb. model	Grid
1	5	0.11	RANS	1
2	5	0.11	LES	2
3	12	0.191	RANS	3
4	12	0.191	LES	4
5	12	0.235	RANS	3
6	12	0.235	LES	4
7	18.5	0.234	RANS	5
8	18.5	0.234	LES	6
9	18.5	0.278	RANS	5
10	18.5	0.278	LES	6
11	18.5	0.22	RANS	5
12	18.5	0.22	LES	6
13	18.5	0.26	RANS	5

Table 3 Mesh characteristics of numerical simulations

	Size of the domain mm	Maximum cell size mm	Local cell size mm	Number of volumes
Grid 1	$500 \times 1000 \times 220$	10	4	$1.3 \cdot 10^6$
Grid 2	$500 \times 1000 \times 220$	5	2	$7.9 \cdot 10^6$
Grid 3	$500 \times 1000 \times 300$	10	4	$1.6 \cdot 10^6$
Grid 4	$500 \times 1000 \times 300$	5	2	$9.8 \cdot 10^6$
Grid 5	$500 \times 1000 \times 320$	10	4	$1.7 \cdot 10^6$
Grid 6	$500 \times 1000 \times 320$	5	2	$10.6 \cdot 10^6$

take into account 2 different cases (see discharge interval in Table 2). These 2 cases with close discharge are also the opportunity to evaluate the sensitivity of discharge with respect of water level.

The grids used in this study corresponded to a 3D unstructured mesh composed of prismatic volumes, which was created by using the open-source version 9.3.0 software SALOME. Because of the cyclic boundary condition applied at the inlet and outlet, special attention was given when building the mesh for these two faces. As required in OpenFOAM, they were built as perfect clones. The grid refinement was based in the meshes used in [9] and [15]. In these references, for similar flow, mesh and time dependence and validation have already been studied. Moreover the cell used here is smaller than those from studies at the same scale [4, 17]. Characteristics of the meshes used in this work are given in Table 3.

The results of the numerical simulations are first compared to experimental ones to be validated. The experimental and calculated flows are shown in Table 4.

The analysis of the flows computed from the experimental water level shows that the calculated flow rate differs from 20 % for the LES simulations (Table 4). We also notice an overestimation of the flow rate with the RANS model especially for steeper transversal slope. Even if the maximum deviation may seem important, we observe that a modification

Table 4 Comparison between measured and computed flow rate Q (m^3/s) for given water depths

Num. case	$S_{lateral}$	h (m)	Q_{exp} (ΔQ_{LES})	Q_{LES}	Q_{RANS}
1, 2	0.050	0.11	0.04 (-23 %) < Q <0.05 (1.4 %)	0.0493	0.0488
3, 4	0.120	0.191	–	0.101	0.114
5, 6	0.120	0.235	–	0.181	0.212
7, 8	0.185	0.234	0.100 (–18 %)	0.118	0.132
9, 10	0.185	0.278	0.180 (–13%)	0.205	0.203
11, 12	0.185	0.220	0.08 (–22%) < Q < 0.1 (2%)	0.098	0.106
13	0.185	0.260	0.17 < Q < 0.18	–	0.179

Errors between experiment and LES simulation are given in parenthesis. If measurements were not done with the same water level than simulation then the discharge measured with the inferior and superior values of the water depth is indicated

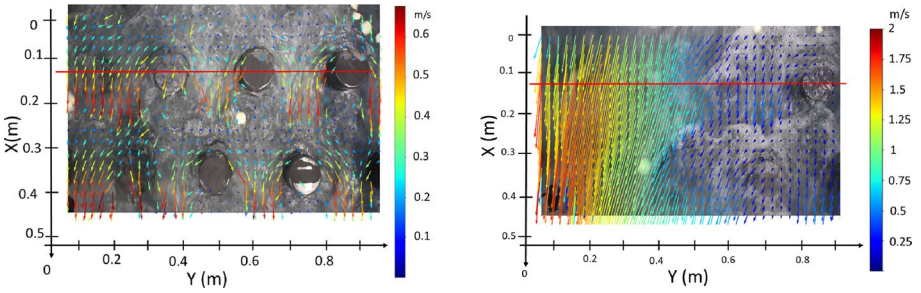

Fig. 4 Measured surface velocity fields for 2 cases: near-emergent case, configuration 3, S = 3%, Q = 60 l/s (left) and submerged case, configuration 3, S = 5%, Q = 180 l/s (right). The red line at X = 0.125 m is used to plot profile on Fig. 5. The arrows are colored by velocity magnitude

of 1–2 cm of the water level is sufficient to find the experimental flow rate (see Table 4 lines 4–6 and 5–7). This variation is of the order of magnitude of the measurement uncertainty, especially since the free surface is not homogeneous on the domain as observed later.

Surface velocity fields obtained by particle tracking are compared to those calculated. The measured fields show two different patterns of flow depending on the submergence of the blocks. When the blocks emerge (left side on Fig. 4) the surface velocities are quite close to what is expected without lateral slope as it will be shown in the last Velocity fields part. When the blocks are submerged (right side on Fig. 4), a transverse component of velocities appears in a part of the domain. To quantify this component, velocity profiles are plotted in Figs. 5 and 6, along the colored lines defined on figure 4.

As for flowrate, at a discharge of 100 l/s, the comparison of the velocity profiles shows that the RANS simulations largely overestimate velocity whereas LES simulations have intermediate values between the simulations with fixed level or flowrate (Fig. 5 left). At a discharge of 180 l/s, when the blocks emerge from water surface, all models provide similar results and reproduce well the measured velocities. The LES simulation remains better to compute the velocity in particular when the block is just submerged (transversal position between 0.2 and 0.4) (Fig. 5 right). LES model is also better to reproduce transversal velocity in the deeper part of the flow (transversal position superior to 0.6 on Fig. 6).

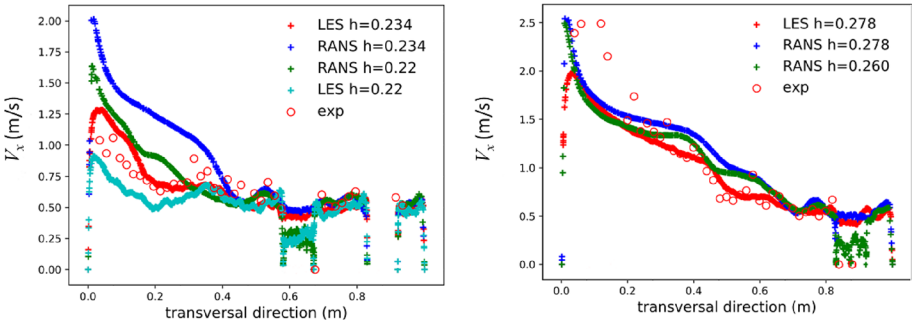

Fig. 5 Profile of axial surface velocity V_x along the red continuous line shown in Fig. 4. The discharge is 100 l/s on the left (numerical cases 7, 8, 11 and 12) and 180 l/s on the right (numerical cases 9, 10 and 13)

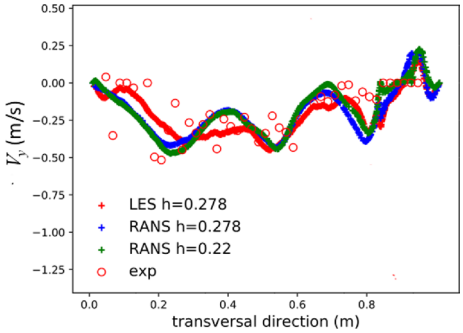

Fig. 6 Profile of transversal surface velocity V_y along the red continuous line shown in Fig. 4. The discharge is 180 l/s (numerical cases 9, 10 and 13)

Given the above and the studies of [9, 15], and [7], the authors consider that the LES model is able to accurately describe the averaged fields in the computational domain.

4 Results and discussion

4.1 Flow pattern analysis

As the calculation of the average velocity is validated, the simulations make it possible to better understand hydrodynamic fields in the whole water domain. The instantaneous values from the LES simulations were averaged over 10 s. Figure 7 shows an emergent case (configuration 2) and a submerged case (configuration 3). For the emergent case, a plunging jet appears between two obstacles with a weak lateral contraction. The velocities in the surface jet are almost uniform (≈ 0.7 m/s) even if it could be noted a stronger value near the obstacles. For the submerged case, the velocity is almost uniform in the longitudinal direction for the largest water level (≈ 1.2 m/s). The longitudinal heterogeneity appears mainly when the obstacles are emergent (Fig. 7 right).

To complete this analysis, the velocity distributions in the transversal planes passing through the obstacles and through the middle of a row of blocks are plotted. Between 2 rows (Fig. 8a), the velocities are equivalent to zero only at the surface whereas the velocity of the jet is almost uniform along the water depth, slower areas correspond to wake

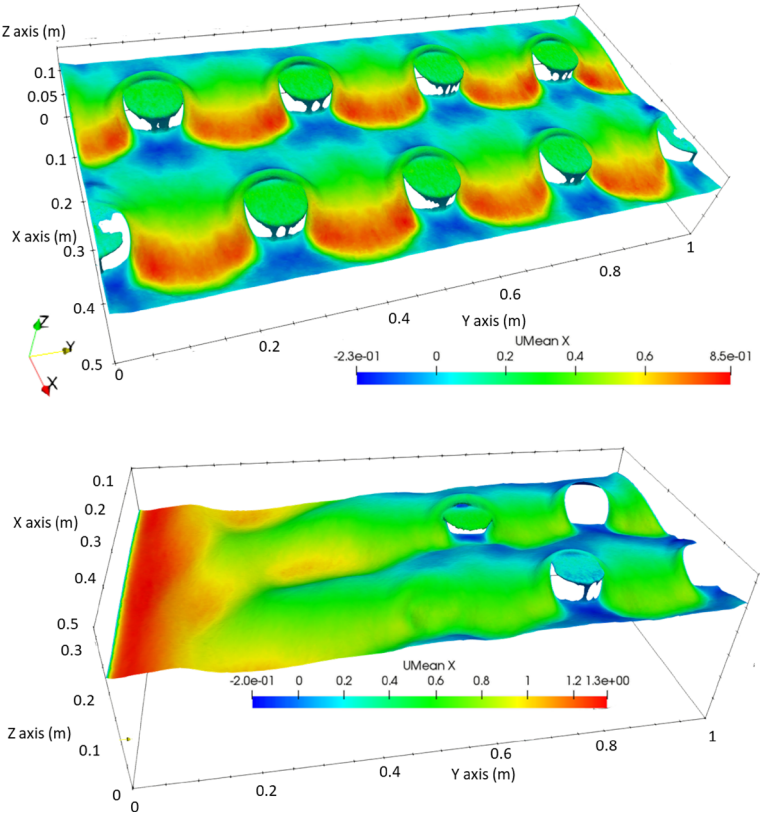

Fig. 7 Free surface coloured by velocity for configuration 2 (top) and configuration 3 (down). Values are averaged over 10 s

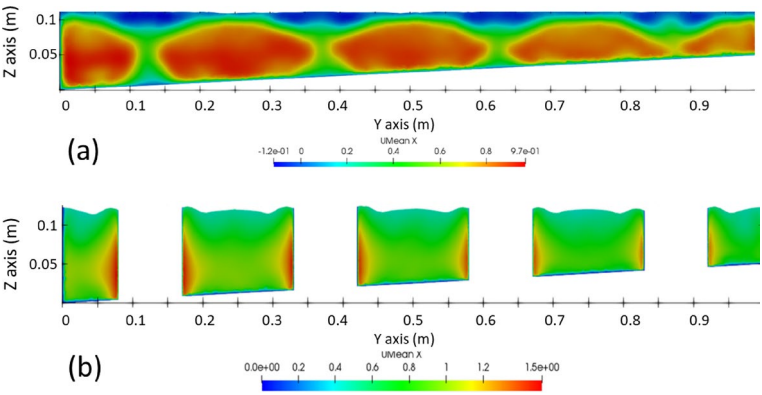

Fig. 8 Longitudinal velocity on a vertical plane for simulation 2 between 2 rows (X = 0.25) **a** and on the block line (X = 0.125) **b**

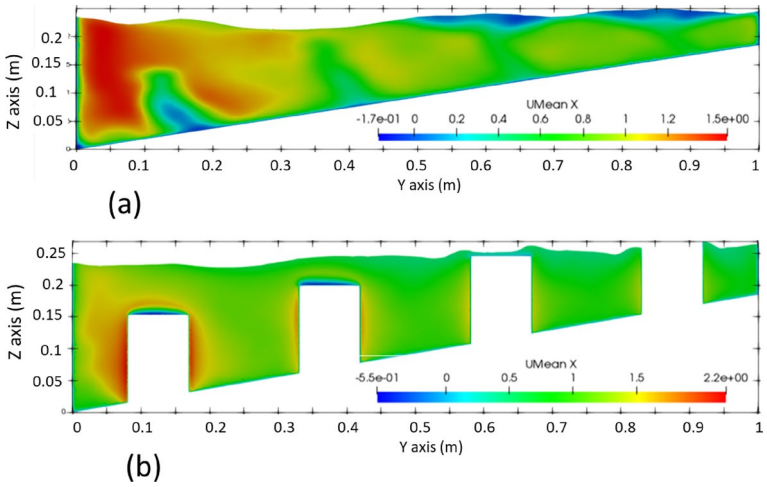

Fig. 9 Longitudinal velocity on a vertical plane for simulation 8 between 2 rows (X = 0.25) **a** and on the line of blocks (X= 0.125) **b**

zone behind blocks. The low velocity at the surface is due to the recirculating zone (Fig. 7) already observed for one block with similar hydrodynamic flow [12]. Between 2 blocks (Fig. 8b), the velocities are also vertically uniform. Near the blocks, the velocity is faster than the averaged value. This acceleration is located on a small area (for instance at $0.3< Y <0.35$) which is not significant for fish passage [21]. The maximum velocity is 1.5 m/s (3.3 m/s at real scale) but most velocities between blocks are lower than 0.8 m/s (1.7 m/s at real scale). These value are similar to the swimming capacity of targeted species (see above). Hence, the computed velocity fields are totally consistent with the previous study with no transversal slope [21]. It was also checked that the turbulent intensity in the jet is still between 20 and 30 % as mentioned in [21].

For the submerged case, we can notice that the shallower flow part (Y > 0.5) (Fig. 9) is similar to the emergent case (Fig. 8). For the deeper part (Y< 0.3), the velocity increases with the distance from the bed and the velocity over the block is faster and uniform. These high velocities provide a higher total discharge which improve the fishway attractiveness. Some negative velocities are computed in the wake because of a recirculation zone near the bed [12]. Only the transition pattern between the 2 cases presents a particular flow pattern ($0.3< Y <0.5$).

To verify if the lateral slope modifies the velocities in the passable part, transverse velocities (V_y) for lateral slopes of 5, 12 and 18.5 % were plotted (Fig. 10). In the plane between 2 rows, the presence of flow jets is clearly visible since V_y having symmetrical and opposite directions. As the lateral slope increases, the flow structure is modified: velocities at the surface are going towards the lower point at the surface and in the opposite direction near the bottom. However, the structure is identical in the emergent zone up for lateral slope up to 12%, and V_y remains inferior to 30 % of the longitudinal velocity. At a lateral 18.5% slope, the flow is significantly influenced by the lateral transfers, and passability could be modified at this plane because of transversal or vertical velocity as shown on Fig. 11. Indeed the results reveal the presence of a transverse flow in the space between blocks. This could prevent the fish passage but the transverse velocity is negligible in the emergent part even for 18.5% slopes.

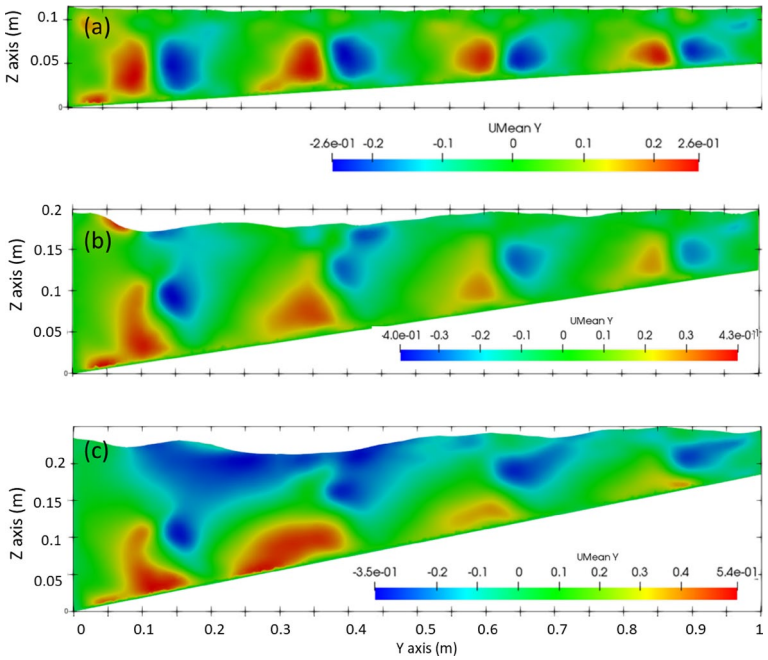

Fig. 10 Transverse velocity for simulation 2 with 5% slope **a**, simulation 4 with 12% slope **b** and simulation 8 with 18.5% slope **c** on a plane between 2 rows (X = 0.25 m)

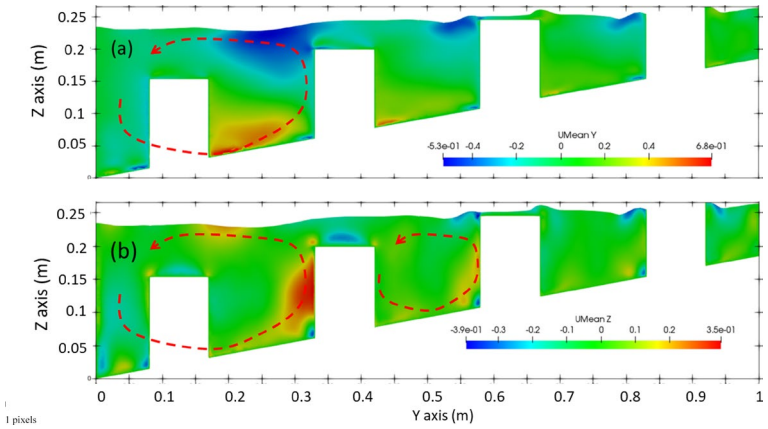

Fig. 11 Transverse velocity **a** and vertical velocity **b** for simulation 8. The red arrows indicate the presence of a rotational structure considering averaged velocity

Finally, simulations indicate that transverse and vertical velocities are identical to flat bottom case in emergent parts. This proves that the fish passage will be mainly conditioned by the longitudinal velocity as already studied.

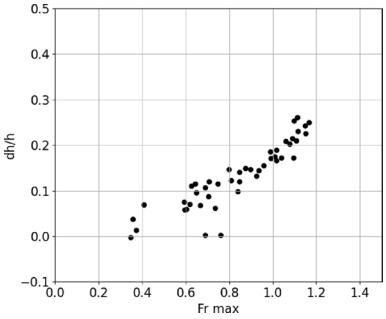

Fig. 12 Variation of free surface dimension between measurements on the left and right pass sides for 2 cases with configuration 3

4.2 Lateral deviation of free surface

The simulations also reveal that the level of the free surface differs on the left and on the right side. To quantify this deviation, the whole series of experiments were used. The variation *dh* is computed as the difference between the averaged water level at the block on the shallower side and the one at the deeper side (Fig. 12).

For a lateral slope of 5 % (configuration 1), the lateral water level difference is about 5 % of the average water depth. For a lateral slope of 18.5 % (configuration 3), the difference increases to 20 % (Fig. 12). This difference seems to correlate well with the Froude number in the deepest zone (Fr_{max}). This Froude number is based on the averaged velocity between blocks obtained with the formulation of [7] applied with the maximal water depth in the transverse direction. The previous analysis confirms that water level inclination could be due to the acceleration caused by the transverse flows. For a real pass with a maximum depth of 1 m with a transversal slope of 18 %, the water level variation between the right and left sides could reach 20 cm. Even if this water surface variation could not change the passability, it was to be considered for stage-discharge relationship as explained further.

4.3 Stage-discharge relationship

This section presents the methodology for designing a fish pass according to the flow rate chosen and a target species. We would like to show that the method induced by the use of the Cassiopee software [11] is valid under certain conditions.

Because of free surface inclination, it seems important to test the influence of the average level used to describe the stage-discharge relationship. Therefore it is used either a water level based on the upstream-downstream difference of the lowest block (deepest flow), or for the highest block (shallowest flow), or for an averaged of the 2 previous values. The calculated flows are obtained with the formula described in [7]. The method is based on a momentum balance on a water volume around each block. To take into account the lateral slope, the water depth is adjusted for each block assuming a constant water level. Then the discharges obtained for each block are summed laterally. This method neglects the transversal fluxes of mass and momentum [8]. For configuration 1, the reference water level used has a low influence because the difference in elevation of the free surface is small between the 2 sides (Fig. 13).

The choice on the reference water level is significant only when the transversal slope is steep (configuration 3). This is due to the existing lateral slope for the free surface. However, the use of an average level (Fig. 14) makes it possible to compensate for the non

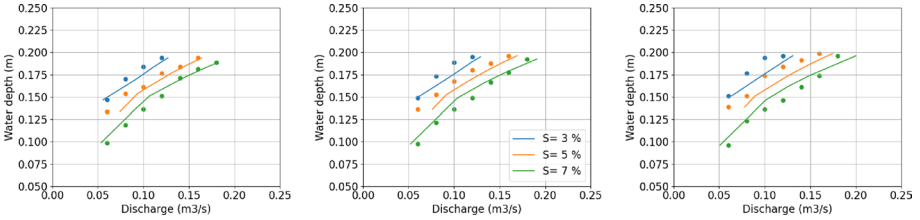

Fig. 13 Stage discharge relationship for configuration 1 as a function of water height considered: low plot (left), average high-low (center), high plot (left). Dots represent measurements and curves are the model [8]. Colors depend on the slope

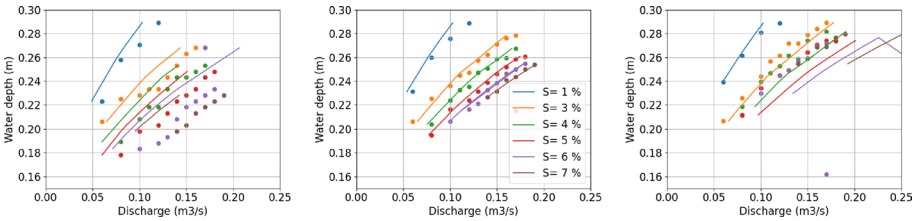

Fig. 14 Stage discharge relationship for configuration 3 as a function of water height considered: low plot (left), average high-low (center), high plot (left). Dots represent measurements and curves are the model [8]. Colors depend on the slope

Fig. 15 Stage discharge relationship for configuration 2. Dots represent measurements and curves are the model [8]. Colors depend on the slope

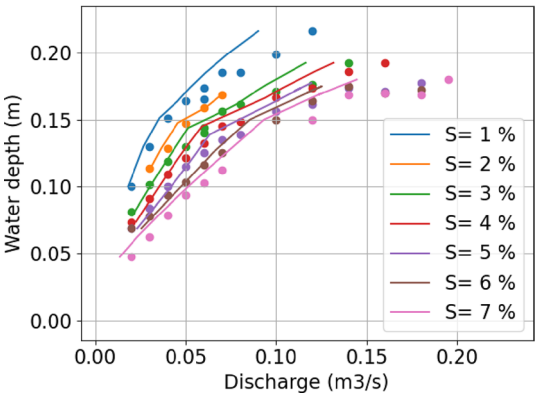

horizontal water surface. The agreement between experiment and calculation is good (less than 10 %) except for the 7 % slope in configuration 1 (Fig. 13). The difference may come from the difficulty to obtain a precise value of the water level when the Froude number is high, especially as the blocks are then slightly submerged. Indeed for a side slope of 18.5 %, the blocks are more largely submerged and the measurement of the level is facilitated.

The validity of the stage-discharge formulas in the submerged case is obtained in particular with configuration 2 (Fig. 15). This configuration minimizes the above-mentioned reference water level problem thanks to a small lateral slope. On the other hand, the constant elevation of the top of the blocks ensures submergence for low discharge. Figure 15 clearly shows a change in the trend when all the blocks are submerged. We observed that

even for high flows, the design formulation [7, 8] allows to estimate correctly the stage-discharge relationship. It is recalled that when no block is submerged (h <13 cm), configurations 1 and 3 are similar. Figure 15 therefore also validates the formula for low flow in configuration 1.

We can therefore conclude that for the estimation of the discharge, the design assumption of low lateral transfers between blocks is valid whatever the transverse slope, at least up to 18.5 %. The main precaution is to use an average water level.

4.4 Maximum velocities assessment

It remains to be verified that the design method described above gives a consistent estimation of the maximum velocity from a classical design based on an average height [11]. Here it focused on experimental configurations 2 and 3 studied by particle tracking velocimetry. This gives a spatial description of the surface velocity field for all tested flow rates and slopes and it allows to verify that the observations made for the simulations are true for all the cases. Two points related to the fish passage are mainly investigated: the absence of important cross flows in the passing area (emergent blocks), and secondly the maximum velocities in these areas.

In the emergent cases, surface velocities in the jet are well oriented along the longitudinal axis as for no transversal slope (Fig. 4). On the other hand for the submerged cases, large lateral velocities towards the lowest point are observed at the surface. It is important to note that this phenomenon is not due to a flow not well-established because it also appears in the numerical simulations where a uniform flow is assumed. This implies transverse velocities in the opposite direction in the lower layers as it is pointed out in the numerical results. Even for high flows and high lateral slopes, these lateral velocities are low in the emergent part which can be passed by fishes. In the submerged zone, the flow towards the low points also corresponds to the structure of the flows provided by the simulations. Moreover, when the flow is strongly submerged, the block arrangement still has influence on the surface velocity. The velocity is slightly higher at the passages above the blocks.

To estimate a maximum surface velocity between each block, the domain is divided into a rectangle in which the maximum velocity (magnitude) is sought. Figure 16 presents these zones and an example of maximal velocity position.

The maximum surface velocities are then compared to those obtained with the formula of [8] and [7] and using the average level. It was chosen to present here a theoretical maximum velocity including submerged flows. Indeed the previous works provide values of maximum velocity only for the emergent cases. For submerged cases, after several tests, it appeared that the most relevant method was to provide the theoretical surface velocity corrected by the obstruction ratio $(1/(1-\sqrt{C})$. This allows to take into account the fact that for low submergence the flow pattern between blocks remains in the upper layer even if for larger water depth a horizontal planar uniformity exists. Therefore the present method maximizes the velocity in the submerged case.

Figure 17 verifies that for the emergent case the maximum velocity estimated by the proposed formulation is relevant. For configuration 2, all cases are almost submerged. Nevertheless, a good agreement with the theoretical formulation for weaker slopes can be also observed, the standard deviation for all experiments is 16 %. For steeper slope ($S = 18.5\%$), the gap between experiments and simulation increases with the discharge. It is due to the difficulty to define an averaged water level with high Froude number and surface deformation. On Fig. 15, the discrepancy between simulation and experiments for submerged flow can also be noticed but they are not suitable for fish passing

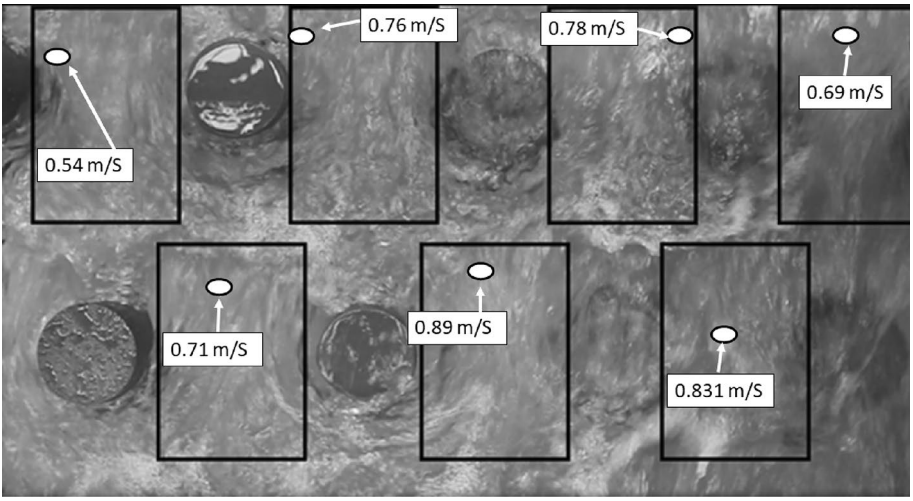

Fig. 16 Search area for maximum and automatic identification of their position for a slope of 4% and Q = 80 l/s

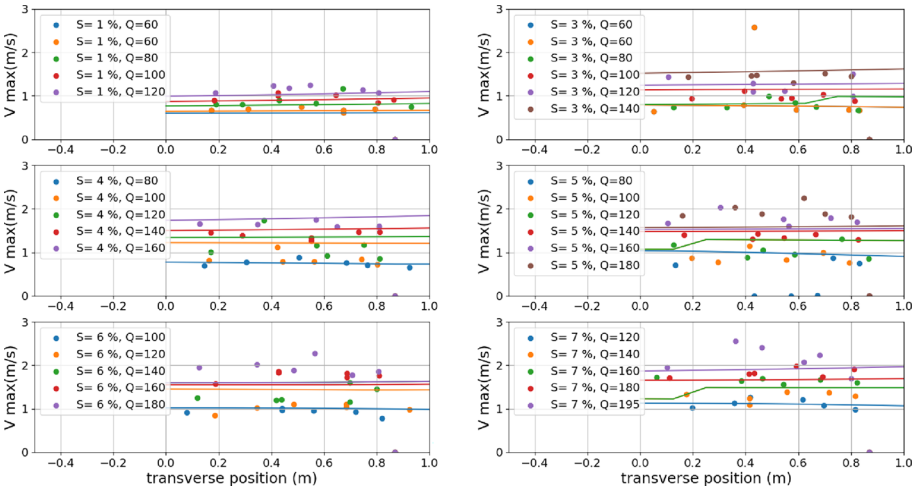

Fig. 17 Cross-sectional profile of maximum measured and calculated velocities for configuration 2. Dots represent measurements and curves are the model [8]

since the maximal velocity is superior to 1.5 m/s (3.3 m/s at real scale) as it can also be observed on Fig. 17. It is interesting to notice that the maximum velocity is almost constant along the channel width. Design formula indicates that the velocity does not depend on the water depth in emergent case without bed roughness. Indeed the velocity does not depend on the lateral slope. In a real channel, bottom roughness can decrease the maximum velocity and thus facilitate the passage in the zones with low water depth [2, 10, 19].

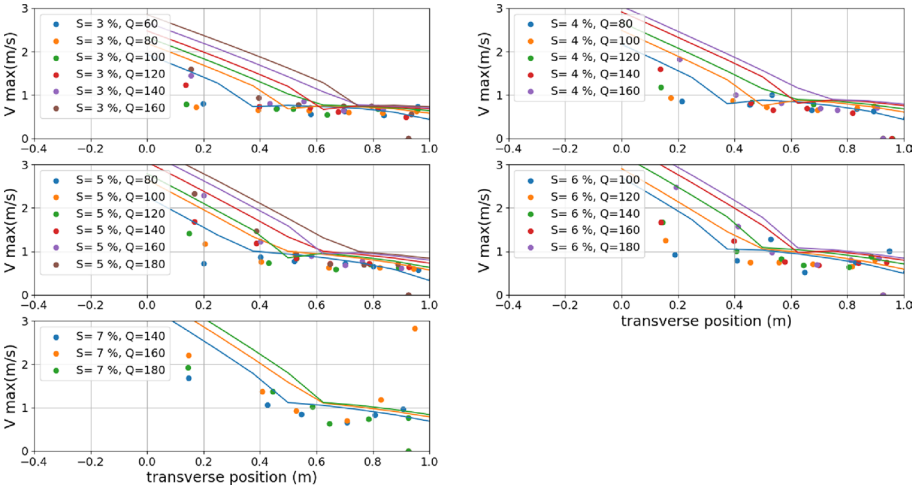

Fig. 18 Cross-sectional profile of maximum measured and calculated velocities for configuration 3. Dots represent measurements and curves are the model [8]

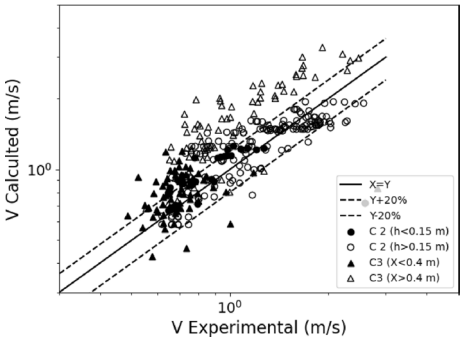

Fig. 19 Comparison of experimental and calculated maximal velocity for configuration 2 (C2) and 3 (C3). Full signs represent emergent cases and open signs are for submerged cases

For configuration 3 (Fig. 18), there is a good agreement between the maximum velocity measured on the surface and the one calculated in the area of emerging blocks. The standard deviation is also 15 % but a bias of 10% can be observed (Fig. 19) for emergent cases. It is a safety margin for the design process. The maximum velocity should not be on the surface but in the middle water depth as observed in experiments [21]. At a given slope and flowrate, in spite of a weak variation of the maximal velocity, the evolution according to the flow and the water height is consistent between measurements and calculations. As already mentioned, the maximum value for the fish passage provided in the submerged case is not easily definable. Nevertheless, the chosen assumption allows to reproduce the influence of the flow and the slopes, while maximizing the velocity (almost 30 % on Fig. 19). Thus, the relationship is safe for designing in order to avoid making a submerged area appear more passable than an emergent area.

5 Conclusion

The rock-ramp fishways with protruding blocks and lateral slope from 5% to 18.5% have been studied numerically and experimentally to verify if lateral transfers induced by lateral slopes have a negative effect on the flow conditions inside the ramp and on its passability by fish. Results revealed that the methodology for assessing stage-discharge relationship and maximum velocities is still relevant whatever the lateral slope. However, as the lateral slope increases, so does the lateral deviation of the free surface, as well as the transverse and vertical velocities in the emergent part of the ramp, near the submerged part. This is why it appears preferable to limit the transversal slope to a 12% maximum in rock-ramp fishways with protruding blocks. This recommendation is already much higher than the one applied up to now in France (lower or equal to the longitudinal slope, so mostly lower or equal to 4% to 6%) and will allow to reduce the width and thus the cost of the ramp. When designing a ramp with a lateral slope, as velocities significantly increase where blocks are submerged, it is recommended to ensure that a passage zone at least 3 times wider than the width of a block is not submerged for the maximum river flow targeted for fish migration.

Acknowledgements The calculations were performed on the Olympe supercomputer at CALMIP, Toulouse, France, which is gratefully acknowledged (Project P20048).

Author contribution LC, FM and DC—wrote the manuscript. LC—computed discharge relationship and analysed results. FM—performed numerical simulations. PL—carried out experiments. All authors reviewed the manuscript.

Declarations

Conflict of interest The authors declare no conflict of interest.

References

1. Amaral SD, Quaresma AL, Branco P, Romão F, Katopodis C, Ferreira MT, Santos AN (2019) Assessment of retrofitted ramped weirs to improve passage of potamodromous fish. Water 11:1–10
2. Amaral SD, Branco P, Romão F, Ferreira MT, Pinheiro AN, Santos JM (2021) Evaluation of low-head ramped weirs for a potamodromous cyprinid: effects of substrate addition and discharge on fish passage performance stress and fatigue. Water 13:765
3. Baki ABM, Zhu DZ, Rajaratnam N (2014) Mean flow characteristics in a rock-ramp-type fish pass. J Hydraul Eng 140:156–168
4. Baki ABM, Zhu DZ, Rajaratnam N (2016) Flow simulation in a rock-ramp fish pass. J Hydraul Eng 142:1–12
5. Baudoin JM, Burgun V, Chanseau M, Larinier M, Ovidio M, Sremski W, Steinbach P, Voegtle B (2014) Assessing the passage of obstacles by fish. Concepts, Design and Application Onema, Paris, France
6. Cassan L, Tien T, Courret D, Laurens P, Dartus D (2014) Hydraulic resistance of emergent macroroughness at large froude numbers: design of nature-like fishpasses. J Hydraul Eng 140:1–9
7. Cassan L, Miranda FC, Laurens P (2023) Hydraulic resistance in rock-ramps fish passes for several shapes of macro-roughness. J Hydraul Eng 149(2):456. https://doi.org/10.1061/JHEND8.HYENG-13096
8. Cassan L, Laurens P (2016) Design of emergent and submerged rock-ramp fish passes. Knowl Manag Aquat Ecosys 417:1–10
9. Chorda J, Cassan L, Laurens P (2019) Modeling steep-slope flow across staggered emergent cylinders: application to fish passes. J Hydraul Eng 145:1–14

10. Chorda J, Larinie M, Thinus Z (2004) A flume study of steep-slope flows above large-scale roughness elements and their applications to fish passes. In: 5th international symposium on ecohydraulics - aquatic habitats: analysis & restoration Madrid, Spain
11. Dorchies D, Chouet M, Grand F, Cassan L, Richard S, Courret D (2022) Cassiopee a software to bridge the gap between researchers and engineers in hydraulic calculations. In: Proceedings of the 39th IAHR world congress, Granada, Spain
12. Ducrocq T, Cassan L, Chorda J, Roux H (2017) Flow and drag force around a free surface piercing cylinder for environmental applications. Environ Fluid Mech 17:629–645
13. Golpira A, Baki AB, Zhu DZ (2020) Higher-order velocity moments, turbulence scales and energy dissipation rate around a boulder in a rock-ramp fish passage. Sustainability 12:5385
14. Larinier M, Courret D, Gomes P (2006) Technical guide to the concept on nature-like fishways. Rapport GHAAPPE RA.06.05-V1, 5
15. Miranda FC, Cassan L, Laurens P, Tran TD (2021) Study of a rock-ramp fish pass with staggered emergent square obstacles. Water 13:1175. https://doi.org/10.3390/w13091175
16. Pang ALJ, Skote M, Lim SY (2016) Modelling high Re flow around a 2D cylindrical bluff body using the k-w (SST) turbulence model. Prog Comput Fluid Dyn Int J 16(1):48–57. https://doi.org/10.1504/PCFD.2016.074225
17. Quaresma AL, Pinheiro AN (2021) Modelling of pool-type fishways flows: efficiency and scale effects assessment. Water 13:851. https://doi.org/10.3390/w13060851
18. Romdhane H, Soualmia A, Cassan L, Masbernat L (2017) Evolution of flow velocities in a rectangular channel with homogeneous bed roughness. Int J Eng Res 6(3):120–125
19. Silva AT, Bermúdez M, Santos JM, Rabuñal JR, Puertas J (2020) Pool-type fishway design for a potamodromous cyprinid in the Iberian Peninsula: the Iberian barbel-synthesis and future directions. Sustainability 12:3387
20. Smagorinsky J (1963) General circulation experiments with the primitive equations: I. The basic experiment. Mon. Weather Rev. 91:99–164
21. Tran TD, Chorda J, Laurens P, Cassan L (2016) Modelling nature-like fishway flow around unsubmerged obstacles using a 2D shallow water model. Environ Fluid Mech 16:413–428